PERGAMON

International Journal of Multiphase Flow 27 (2001) 577–598

International Journal of Multiphase Flow

www.elsevier.com/locate/ijmulflow

Steady and unsteady flow in a heated capillary

Y.P. Peles, L.P. Yarin, G. Hetsroni *

Department of Mechanical Engineering, Technion-Israel Institute of Technology, 32000 Haifa, Israel

Received 28 June 1999; received in revised form 29 June 2000

Abstract

This paper deals with forced fluid flow in heated micro-channels with a distinct evaporation front. A simple one-dimensional model of the flow is proposed. The effect of a number of dimensionless parameters such as *Pe*, *Ja*, and dimensionless heat flux, on the velocity, temperature and pressure within the liquid and vapor domains has been studied, and the parameters corresponding to the steady flow regimes as well as the domains of flow instability are delineated. An experiment was conducted and demonstrated that the flow in micro-channels appears to have two distinct phase domains, one for the liquid and the other for the vapor, with a very short section of two-phase mixture between them. © 2001 Elsevier Science Ltd. All rights reserved.

1. Introduction

Recently, increasing interest has been focused on new methods for cooling of electronic components which have high power densities. One of the promising methods of cooling these components are single- or two-phase convective flows through micro-channels (Peng and Wang, 1998; Incropera, 1999). The developments in the semiconductor technology have made possible miniaturization, which allows for the manufacturing of micro-heat-exchangers consisting of multiple minute flow conduits with hydraulic diameter ranging from 10 to 1000 μm. These micro-heat-exchangers are characterized by extremely high surface area per unit volume, low thermal resistance, low mass, volume and inventory of the working fluid.

The investigations of fluid flow in micro-channels may be divided into two groups: (i) single-phase flow (ii) evaporative two-phase flow. Single-phase flow was extensively investigated following Tukermann and Pease (1981). Two-phase flow is much less understood.

* Corresponding author. Tel.: +972-4-829-2058; fax: +972-4-832-4533.
E-mail address: hetsroni@techunix.technion.ac.il (G. Hetsroni).

0301-9322/01/$ - see front matter © 2001 Elsevier Science Ltd. All rights reserved.
PII: S0301-9322(00)00041-0

Hsu (1962) developed a semitheoretical model that provides considerable insight into the effects of a non-uniform liquid superheat resulting from transient conduction in the liquid during the bubble growth and release process. The model shows that there is a finite range of active cavity sizes on the heating surface, which depends on subcooling, pressure, heat flux and physical properties of the flow. For water at atmospheric pressure, temperature difference between the wall and saturation temperatures is around 15.6°C, thermal boundary layer thickness of 76 μm near the nucleation site, and heat flux of 30 W/cm^2, the active nucleation sites are those having cavity opening of radius 2.5–15 μm. The thermal boundary layer far from the nucleation site was measured by optical means by Yamagata et al. (1955). It was found that the thickness of the thermal boundary layer is of the order of 250 μm. Thus the boundary layers of an adjacent heated micro-channel walls converge in a channel with a hydraulic diameter on the order of 100 μm, causing a higher bulk temperature and therefore a wider range of active nucleation sites. The latter results in higher bubble departure frequency. Furthermore, the bubble departure diameter in channels of regular size is of the order of 1 mm, indicating that the bubble initiation process in micro-channels is strongly controlled by the surrounding walls.

Peng and Wang (1993) investigated the flow boiling through micro-channels with a cross-section of 0.6×0.7 mm^2. They observed that no partial nucleate boiling existed and that the velocity and liquid subcooling have no obvious effect on the flow nucleate boiling fluid. (Peng and Wang (1994a,b, 1996)) conducted additional experimental investigations on flow boiling in micro-channels with rectangular cross-sections ranging from 0.1×0.3 to 0.6×0.7 mm^2. Peng et al. (1998) suggested a dimensionless parameter for nucleate boiling in micro-channels, which agree well with the experimental data.

Bowers and Mudawar (1994) performed an experimental study of pressure drop and critical heat flux (CHF) in mini-channels with circular cross-section ($d = 2.54$ mm and $d = 510$ μm) using R-113. A CHF correlation proposed by Katto (1978) was presented as $q_{\mathrm{CHF}}/Gh_{\mathrm{L,G}} = 0.16We_*^{-0.19}(L/D)^{-0.54}$, where q_{CHF} is the critical heat flux, G the mass velocity, L the channel length, D the channel hydraulic diameter, $h_{\mathrm{L,G}}$ the latent heat of vaporization and We_* is the Weber number defined as $We_* = \sigma/(\rho_{\mathrm{L}}u^2L)$, where σ is the surface tension (N/m), ρ_{L} the liquid density (kg/m^3) and u is the inlet velocity (m/s). As the channel size decreases, the capillary forces acting in the longitudinal direction become significant. The experiment yields CHF values about 200 W/cm^2. However, the pressure drop for the mini-channels were less than 1 KPa compared to 23 KPa for the micro-channels.

Peles et al. (1998) developed a one-dimensional model for a two-phase laminar flow in a heated capillary, moved by liquid evaporation at the interface. The approach allows to estimate the effect of capillary, inertia, frictional and gravity forces on the shape of the interfacial surface as well as the velocity and temperature distribution. They also demonstrated that at Euler numbers larger than 10^8 a self-regulated regime of flow can be realized. A two-dimensional model of steady state evaporation of liquid–vapor meniscus in a heated capillary slot was considered by Khrustalev and Faghri (1995).

The aim of the present work is to study the steady, forced flow in a heated micro-channel with a distinct evaporation front. The calculation is based on a simplified one-dimensional model of flow with flat evaporation front dividing the liquid and vapor into two different domains. Specifically, we consider the conditions corresponding to the existence of steady flow with evaporation front. The knowledge of such conditions is necessary to designing cooling systems of electronic devices

with high power densities, choosing operating parameters ensuring their stability, etc. Our results are probably restricted to high rates of evaporation in long enough micro-channels.

2. The physical model

Evaporative two-phase flow in a heated micro-channel resembles a two-phase slug flow with distinct domains of liquid and vapor. These domains are divided by the infinitely thin evaporating front, which propagates relatively to the fluid with a velocity u'_f equal (numerically) the linear rate of liquid evaporation. In the frame of reference associated with micro-channel walls, the velocity of the evaporation front is

$$u_f = |u_L| - |u'_f|, \tag{1}$$

where u_f and u'_f are the velocity of the evaporating front in the systems of coordinates associated with the micro-channel wall and the fluid flow, respectively, and u_L is the liquid velocity in an inertial system of coordinate.

Depending on the correlation between u'_f and u_L, the evaporation front moves downstream ($|u'_f| < |u_L|$) or upstream ($|u'_f| > |u_L|$) (Fig. 1). Essentially, in both cases the flow in the micro-channel is unsteady. At the same time, at certain combination of governing parameters (initial velocity of liquid, heat flux on the wall, etc.) the regime of flow may be steady. It corresponds to the kinematic condition $u'_f = u_L$ which determines fixed position of evaporation front in the micro-channel as well as invariable length of the "liquid" and "vapor" domains. The velocity, temperature and pressure distributions corresponding to such a flow are plotted in Fig. 2. The velocity of the vapor increases monotonically along the channel axis, whereas the liquid velocity is

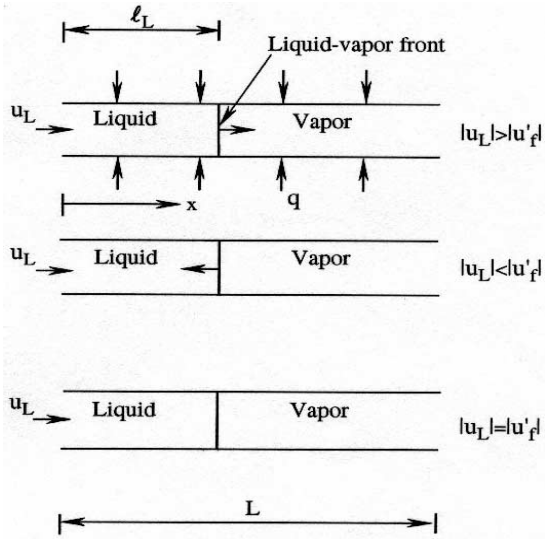

Fig. 1. The scheme of the flow in a heated capillary. u_L is the liquid velocity and u'_f is the front velocity relative to the liquid. ℓ_L is the liquid length domain and L is the total channel length.

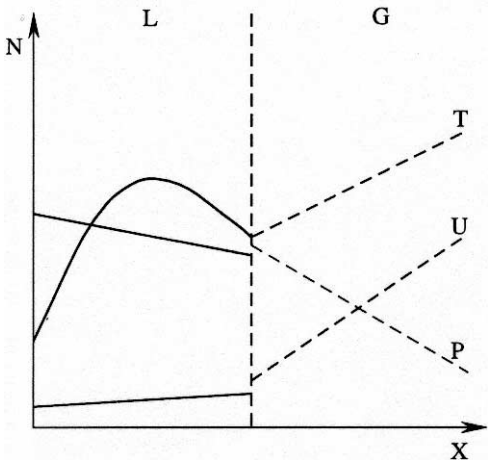

Fig. 2. The velocity, temperature and pressure distributions along the axis of a heated capillary ($N = u, T, P$), G and L correspond to vapor and liquid domains, respectively. Solid line: liquid domain; dotted line: vapor domain (concave meniscus).

almost constant. The latter is a result of low thermal expansion of the liquid: $\gamma = 0.18 \times 10^{-3}$ K^{-1} for water at $t = 20$°C (Kuchling, 1980) and $\rho_{\mathrm{L}}(T_{\mathrm{L}}) \approx$ constant at 20°C $< t <$ 100°C. Accordingly, within such a range of temperature the change of liquid velocity does not exceed 4%.

At the evaporation front there is a jump in the flow velocity which equals to $\Delta u = u_{\mathrm{L}}(\rho_{\mathrm{L,G}} - 1)$, where $\rho_{\mathrm{L,G}} = \rho_{\mathrm{L}}/\rho_{\mathrm{G}}$, ρ_{L} and ρ_{G} are the liquid and vapor densities, respectively. Since $\rho_{\mathrm{L,G}} \gg 1$ a jump in the flow velocity expresses approximately as $\Delta u \simeq u_{\mathrm{L}}\rho_{\mathrm{L,G}}$. The temperature distribution has a characteristic maximum within the liquid domain, which is located in the vicinity of the evaporation front. Such a maximum results from two opposite factors: (i) heat transfer from the hot wall to the liquid, and (ii) heat removal due to the liquid evaporation at the evaporation front. The pressure drops monotonically in both domains and there is a pressure jump at the evaporation front due to the surface tension and phase change effect on the liquid–vapor interface.

Taking into account the above-mentioned factors it is possible to present the stationary flow in a heated capillary as a flow of liquid and its vapor divided by an infinitely thin evaporation front. The parameters of these flows are related to each other by the condition of mass, momentum and energy conservation at the evaporation front.

To describe the flow in a heated capillary we use the mass, momentum and energy balance equations. At moderate velocity, the effects due to compressibility of liquid and vapor as well as energy dissipation in gaseous and liquid phases are negligible. Assuming that thermal conductivity and viscosity of the vapor and the liquid are independent of temperature and pressure, we arrive at the following system of equations:

$$\mathrm{div}(\rho_i \mathbf{v}_i) = 0, \tag{2}$$

$$\rho_i \mathbf{v}_i \nabla h_i = \lambda_i \nabla^2 T_i, \tag{3}$$

$$\rho_i (\mathbf{v}_i \nabla)\mathbf{v}_i = -\nabla P_i + \mu_i \nabla^2 \mathbf{v}_i, \tag{4}$$

where $\rho, \mathbf{v}, T$ and h are the density, velocity, temperature and enthalpy (vector $\mathbf{v}$ has components u, v, w which are directed along axis x, y, z, respectively), P the pressure, λ and μ the thermal conductivity and viscosity, respectively, ∇ and ∇^2 are the gradient and the Laplace operator; $i = \mathrm{G}, \mathrm{L}$ corresponds to vapor and liquid.

The system of Eqs. (2)–(4) should be supplemented by relations determining the dependencies $P_{\mathrm{G}}(\rho_{\mathrm{G}} T_{\mathrm{G}}), \rho_{\mathrm{L}}(T_{\mathrm{L}})$ and $h_i(T_i)$.

At steady flow in a heated micro-channel the conditions at the evaporation front may be expressed by the of continuity of mass, thermal fluxes on the interphase surface and the equilibrium of all acting forces (Landau and Lifshitz, 1959). With reference to the evaporative meniscus the balance equations have the following form (Peles et al., 1998):

$$\sum_{i=1}^{2} \rho_i v_i n_i = 0, \tag{5}$$

$$\sum_{i=1}^{2} \left(\rho_i v_i h_i + \lambda_i \frac{\partial T_i}{\partial x_i} \right) n_i = 0, \tag{6}$$

$$\sum_{i=1}^{2} (P_i + \rho_i v_i v_k) n_i = \left(\mu_{ik}^{(2)} - \mu_{ik}^{(1)} \right) n_k + \sigma \left(r_1^{-1} + r_2^{-1} \right) n_i + \frac{\partial \sigma}{\partial x_i}, \tag{7}$$

where σ is the surface tension, μ_{ik} the tensor of viscous tension; $v_i n_i$ and $(\partial T_i / \partial x_i) n_i$ the normal component of the velocity vector and interphase surface gradient, respectively, r_1 and r_2 the general curvature radii of the interphase surface, n_i and n_k correspond to the normal and tangent directions; $n_i^{(1)} = -n_i^{(2)}$, $i = 1$ (G), $i = 2$ (L), $x_i = x, y, z$.

The radius of curvature r of the meniscus and its depth H express for cylindrical micro-channel as

$$r = r_0 / \cos\theta, \tag{8}$$

$$H = r_0 (1 - \sin\theta) / \cos\theta, \tag{9}$$

where r_0 and θ are the radius of the micro-channel and the contact angle, respectively.

When the contact angle is close to $\pi/2$ (for example, for the system water/steel $\theta \sim 0.45\pi$) , the ratio H/r_0 is small, we estimate the order of magnitude of the terms in Eqs. (2)–(4) and conditions (5)–(7). Choosing in the meniscus as characteristic scales of length in the longitudinal and transversal directions H and r_0, respectively, we obtain

$$\frac{\partial}{\partial x} \sim \frac{1}{H}, \quad \frac{\partial}{\partial y} \sim \frac{1}{r_0}; \quad \frac{\partial^2}{\partial x^2} \sim \frac{1}{H^2}, \quad \frac{\partial^2}{\partial y^2} \sim \frac{1}{r_0^2}. \tag{10}$$

From Eq. (10):

$$\frac{\partial^2}{\partial x^2} \gg \frac{\partial^2}{\partial y^2}, \tag{11}$$

$$\nabla^2 = \frac{\partial^2}{\partial x^2} + \frac{1}{y} \frac{\partial}{\partial y} \left(y \frac{\partial}{\partial y} \right) \approx \frac{\partial^2}{\partial x^2}. \tag{12}$$

The components of velocity at the meniscus surface are connected with each other (at $\rho_L/\rho_G \gg 1$) by the relation

$$v/u \approx \tan\varphi, \tag{13}$$

where $0 < \varphi < \pi/2 - \theta$, $\tan\varphi = dy^*/dx^*$, $y^*(x^*)$ is the equation which determines the meniscus shape.

At large contact angle (practically $\theta \geqslant 0.4\pi$) the following are valid

$$u > v, \quad u\frac{\partial}{\partial x} \gg v\frac{\partial}{\partial y}. \tag{14}$$

Estimates (12) and (14) allow to reduce the problem on flow in a heated micro-channel to solving the system one-dimensional mass, momentum and energy balance equations. They have the following form:

$$\frac{d\rho_i u_i}{dx} = 0, \tag{15}$$

$$\rho_i u_i \frac{du_i}{dx} = -\frac{dP_i}{dx} - \frac{dF_i}{dx}, \tag{16}$$

$$\rho_i u_i c_{pi} \frac{dT_i}{dx} = \lambda_i \frac{d^2 T_i}{dx^2} + q, \tag{17}$$

where ρ, u, T and P are the density, velocity, temperature and pressure, F the drag force accounting for the effect of viscosity and c_p and λ are the heat capacity and thermal conductivity, respectively, q is the heat flux per unit axial length from the wall.

The boundary conditions for the present problem are:

$$\text{At } x = 0, \quad \rho_L = \rho_{L,0}, \ u_L = u_{L,0}, \ T_L = T_{L,0}, \tag{18}$$

$$\text{At } x = \ell_L, \quad \rho_i = \rho_{i,s}, \ u_i = u_{i,s}, \ P_i = P_{i,s}, \ T_i = T_s, \tag{19}$$

$$\text{At } x = L, \quad \rho_G = \rho_{G,00}, \ u_G = u_{G,00}, \ \frac{dT_G}{dx} = 0, \tag{20}$$

where $L = \ell_G + \ell_L$ is the total length of the micro-channel, ℓ_G and ℓ_L the length of the vapor and liquid regions, respectively, subscripts 0 and 00 correspond to the inlet and outlet cross-section, respectively and s to the evaporation front.

We supplement system (15)–(17) by the equation of state of the vapor and liquid

$$P_G = R\rho_G T_G, \tag{21}$$

$$\rho_L = \rho_L(T_L) \tag{22}$$

by the equation for the vapor pressure at the interphase

$$P_s = P_s(T_s) \tag{23}$$

and by the mass and thermal balances at the evaporation front

$$u_{G,s} = u_{L,s}\rho_{L,G}, \tag{24}$$

$$-\lambda_L\left(\frac{dT_L}{dx}\right)_{x=\ell_L} + \lambda_G\left(\frac{dT_G}{dx}\right)_{x=\ell_L} = h_{L,G}\rho_{L,s}u_{L,s}, \tag{25}$$

where R is the gas constant.

The momentum balance equation at the evaporation front has (neglecting the effect of viscous tension and changing surface tension along of meniscus) the following form:

$$\Delta P = \frac{\sigma}{2r_0}\cos\theta + \rho_{L,s}v_{L,s}^2(1-\rho_{L,s}/\rho_{G,s}), \tag{26}$$

where $\Delta P = P_{G,s} - P_{L,s}$, and $v_{L,s}$ is the linear rate of evaporation.

The linear rate of evaporation (cylindrical micro-channel), may be estimated as follows:

$$v_{L,s} = \frac{4q^*}{h_{L,G}\rho_{L,s}}\frac{L}{d}, \tag{27}$$

where q^* is the heat flux at the wall, $h_{L,G}$ is the latent heat of evaporation.

Using Eqs. (25) and (26) we estimate the contribution of the surface tension in the pressure jump at the evaporation front, for the following parameters: $L/d = 10^2$, $d = 2\times10^{-4}$ m, $\rho_L = 10^3$ kg/m^3, $\rho_L/\rho_G = 10^3$, $h_{L,G} = 2.26\times10^6$ J/kg, $\theta = 80°$, $\sigma = 500\times10^{-4}$ N/m by calculating the ratio of the first term in RHS of Eq. (25) to the second one at $q^* = (3, 30, 300)\times10^4$ W/m^2. As a result we find that the ratio $\sigma\cos\theta/2r_0\rho_L v_L^2(\rho_L/\rho_G)$ equals 1.39, 0.0139, 0.000139, respectively, for $q^* = (3, 30, 300)\times10^4$ W/m^2 It is seen that the pressure jump in a flow in a micro-channel with evaporation front is determined mainly by the phase change. The effect of surface tension shows only at small heat fluxes at the wall. The latter is typical to any system fluid/wall, in particular, for water/glass system with $\theta = 0$. In this case the ratio $\sigma\cos\theta/2r_0\beta\rho_L v_L^2(\rho_L/\rho_G)$ equals 8.93, 0.0893, 0.000893 for $q^* = (3, 30, 300)10^4$ W/m^2.

The above-mentioned estimates show that at high power densities, characteristic for cooling systems of electronic devices, it is possible to neglect the effects due to curvature of the interphase and present it as a flat front.

We add to Eqs. (15)–(17) and (21)–(25) the total mass and energy balances to determine the vapor velocity and the temperature at the outlet cross-section

$$\rho_{G,00}u_{G,00} = \rho_{L,0}u_{L,0}, \tag{28}$$

$$Q_0 + \rho_{L,0}u_{L,0}c_{pL}(T_s - T_{L,0}) + \rho_{L,0}u_{L,0}h_{L,G} + \rho_{L,0}u_{L,0}c_{pG}(T_{G,00} - T_s) = qL, \tag{29}$$

where $Q_0 = \lambda_L(dT/dx)|_{x=0}$ is the upstream heat losses from the liquid in the inlet cross-section.

3. Distribution along the micro-channel

Using system (15)–(17) we determine the distribution of velocity, temperature and pressure within the liquid and vapor domains. We render the equations dimensionless by the following

characteristic scales: $u_{L,0}$ for velocity, $T_{L,0}$ for temperature, $\rho_{L,0}$ for density, $P_{L,0}$ for pressure, $\rho_{L,0}u_{L,0}^2$ for the drag force and L for length

$$\overline{u}_i = u_i/u_{L,0}, \quad \overline{T}_i = T_i/T_{L,0}, \quad \overline{P}_i = P_i/P_{L,0}, \quad \overline{\rho}_i = \rho_i/\rho_{L,0}, \quad \overline{F}_i = F_i/\rho_{L,0}u_{L,0}^2,$$
$$\overline{x} = x/L. \tag{30}$$

The dimensionless equations take the following form:

$$\frac{\mathrm{d}\overline{\rho}_i\overline{u}_i}{\mathrm{d}\overline{x}} = 0, \tag{31}$$

$$\frac{\mathrm{d}\overline{\rho}_i\overline{u}_i^2}{\mathrm{d}\overline{x}} = -Eu\frac{\mathrm{d}\overline{P}_i}{\mathrm{d}\overline{x}} - \frac{\mathrm{d}\overline{F}_i}{\mathrm{d}\overline{x}}, \tag{32}$$

$$\frac{\mathrm{d}\overline{T}_i}{\mathrm{d}\overline{x}} = \frac{1}{Pe_i}\frac{\mathrm{d}^2\overline{T}_i}{\mathrm{d}\overline{x}^2} + \vartheta_i, \tag{33}$$

where $Eu = P_{L,0}/\rho_{L,0}u_{L,0}^2$ is the Euler number, $Pe_i = u_{L,0}L/\alpha_i$ the Peclet number, $\alpha_i = \lambda_i/\rho_{L,0}c_{pi}$ the thermal diffusivity, $\vartheta_i = qL/\rho_{L,0}u_{L,0}c_{pi}T_{L,0}$ is the dimensionless heat flux at the wall.

The boundary conditions for system (31)–(33) are

$$\text{At } \overline{x} = 0, \quad \overline{\rho}_L = 1, \ \overline{u}_L = 1, \ \overline{T}_L = 1, \tag{34}$$

$$\text{At } \overline{x} = \overline{\ell}_L, \quad \overline{\rho}_i = \overline{\rho}_{i,s}, \ \overline{u}_i = \overline{u}_{i,s}, \ \overline{T}_i = \overline{T}_s, \ P_i = \overline{P}_{i,s}, \tag{35}$$

$$\text{At } \overline{x} = 1, \quad \overline{\rho}_G = \overline{\rho}_{G,00}, \ \overline{u}_G = \overline{u}_{G,00}, \ \frac{\mathrm{d}\overline{T}_G}{\mathrm{d}\overline{x}} = 0. \tag{36}$$

The additional equations (21) and (23) and conditions (24) and (29) take the following dimensionless form:

$$\overline{P}_i = R_*\overline{\rho}_G\overline{T}_G, \tag{37}$$

$$\overline{Ps} = \overline{P}_s(\overline{T}_s), \tag{38}$$

$$\rho_L = \rho_L(\overline{T}_L), \tag{39}$$

$$\overline{u}_{G,s} = \overline{u}_{L,s}\rho_{L,G}, \tag{40}$$

$$-\left(\frac{\mathrm{d}\overline{T}_L}{\mathrm{d}\overline{x}}\right)_{\overline{\ell}_L} + \lambda_{G,L}\left(\frac{\mathrm{d}\overline{T}_G}{\mathrm{d}\overline{x}}\right)_{\overline{\ell}_L} = Ja \cdot Pe_L, \tag{41}$$

$$Eu\Delta\overline{P} = We^{-1}\cos\theta + (1-\overline{\rho}), \tag{42}$$

$$\overline{\rho}_{G,00}\overline{u}_{G,00} = 1, \tag{43}$$

$$\overline{Q}_0 + (\overline{T}_s - 1) + Ja + c_{pG,L}\left(\overline{T}_{G,00} - \overline{T}_s\right) = \vartheta_L, \tag{44}$$

where $\overline{Q}_0 = Q_0/(\rho_{\mathrm{L},0} u_{\mathrm{L},0} c_{\mathrm{pL}} T_{\mathrm{L},0})$, $Ja = h_{\mathrm{L,G}}/c_{\mathrm{pL}} T_{\mathrm{L},0}$ is the Jacob number,

$$\vartheta_{\mathrm{L}} = qL/(\rho_{\mathrm{L},0} u_{\mathrm{L},0} c_{\mathrm{pL}} T_{\mathrm{L},0}), \quad R_* = R\frac{\rho_{\mathrm{L},0} T_{\mathrm{L},0}}{P_{\mathrm{L},0}}, \quad c_{\mathrm{pG,L}} = c_{\mathrm{pG}}/c_{\mathrm{pL}}, \quad \lambda_{\mathrm{G,L}} = \lambda_{\mathrm{G}}/\lambda_{\mathrm{L}},$$

$$\overline{\rho} = \rho_{\mathrm{L}}/\rho_{\mathrm{G}}, \quad We = \frac{2r_0 \rho_{\mathrm{L}} v_{\mathrm{L}}^2}{\sigma}.$$

At large Euler numbers when $\Delta\overline{P} \ll 1$ the vapor pressure may be calculated by the Claperon–Clausius equation. In this case $\overline{P}_{\mathrm{s}}$ and $\overline{T}_{\mathrm{s}}$ in Eq (38) correspond to the saturation parameters.

Integrating (31) and (33) we obtain:

$$\overline{\rho}_i \overline{u}_i = 1, \tag{45}$$

$$\overline{T}_i = C_1^{(i)} + \vartheta_i(\overline{x} + Pe_i^{-1}) + C_2^{(i)} \exp(Pe_i \overline{x}), \tag{46}$$

where the constants $C_1^{(i)}$ and $C_2^{(i)}$ express as:

$$C_1^{(\mathrm{L})} = (1 - C_2^{(\mathrm{L})}) - \vartheta_{\mathrm{L}}/Pe_{\mathrm{L}}, \tag{47}$$

$$C_2^{(\mathrm{L})} = [(\overline{T}_{\mathrm{s}} - 1) - \vartheta_{\mathrm{L}} \overline{\ell}_{\mathrm{L}}]/[\exp(Pe_{\mathrm{L}} \overline{\ell}_{\mathrm{L}}) - 1], \tag{48}$$

$$C_1^{(\mathrm{G})} = \overline{T}_{\mathrm{s}} - \vartheta_{\mathrm{G}}\left(\overline{\ell}_{\mathrm{L}} + Pe_{\mathrm{G}}^{-1}\right) - C_2^{(\mathrm{G})} \exp(Pe_{\mathrm{G}} \overline{\ell}_{\mathrm{L}}), \tag{49}$$

$$C_2^{(\mathrm{G})} = -\vartheta_{\mathrm{G}}/(Pe_{\mathrm{G}} \exp Pe_{\mathrm{G}}). \tag{50}$$

The temperature distribution has a maximum at

$$\overline{x}_{\mathrm{m}} = Pe_i^{-1} \ln\left[-\frac{\vartheta_i}{Pe_i C_2^{(i)}}\right]. \tag{51}$$

Such a maximum exists only if $C_2^{(i)} < 0$ and $|C_2^{(i)}| \geqslant 1$. Since ϑ_{G} and Pe_{G} are positive, $C_2^{(i)} < 0$. It is easy to show that $C_2^{(\mathrm{L})}$ is also less than unity at any values of the operation parameters. Taking into account expressions (48) and (50) we obtain from (51) the following:

$$\overline{x}_{\mathrm{m_L}} = Pe_{\mathrm{L}}^{-1} \ln\frac{\vartheta_{\mathrm{L}}[\mathrm{e}^{Pe_{\mathrm{L}}\overline{\ell}_{\mathrm{L}}} - 1]}{[\vartheta_{\mathrm{L}} \overline{\ell}_{\mathrm{L}} - (\overline{T}_{\mathrm{s}} - 1)] Pe_{\mathrm{L}}}, \tag{52}$$

$$\overline{x}_{\mathrm{m_G}} = 1. \tag{53}$$

Thus the maximum of the vapor ($\overline{x}_{\mathrm{m_G}}$) and liquid ($\overline{x}_{\mathrm{m_L}}$) temperatures are located at the outlet cross-section of the micro-channel, and in front of the evaporation front (inside of the liquid domain), respectively.

Consider the pressure distribution in the liquid and vapor domains and taking into account that the drag force F_i takes the form:

$$F_i = \frac{\xi}{2Re_{\mathrm{L},0}} \rho_{\mathrm{L},0} u_{\mathrm{L},0}^2 \int_{0,\overline{\ell}_{\mathrm{L}}}^{\overline{x}} \overline{v}_i \, \mathrm{d}\overline{x}, \tag{54}$$

we obtain from Eq. (32) the following expressions for the liquid P_L and P_G pressures:

$$P_L = 1 - Eu^{-1}\left\{(\overline{\rho}_L - 1) + \frac{\xi}{2Re_{L,0}}\int_0^{\overline{x}} \overline{v}_L \, d\overline{x}\right\}, \tag{55}$$

$$\overline{P}_G = \overline{P}_{G,s} - Eu^{-1}\left\{(\overline{\rho}_{G,s} - 1)/\overline{\rho}_{G,s,0} + \frac{\xi}{2Re_{L,0}}\int_{\overline{\ell}_L}^{\overline{x}} \overline{v}_G \, d\overline{x}\right\}, \tag{56}$$

where $\overline{v}_i = v_i/v_{L,0}$, $\overline{\rho}_L = \rho_{L,0}/\rho_L$, $\overline{\rho}_{G,s} = \rho_{G,s}/\rho_G$, $\overline{\rho}_{G,s,0} = \rho_{G,s}/\rho_{L,0}$, $\overline{x} = x/d$, d is hydraulic diameter of the micro-channel, $\xi = 64$ for laminar flow.

Bear in mind that ρ_L is a weak function of the temperature, such that $\overline{\rho}_L$ is close to unity, we can write approximate expression of $\overline{P}_L$

$$\overline{P}_L \simeq \frac{\xi}{2Re_{L,0}} Eu \int_0^{\overline{x}} \overline{v}_L \, d\overline{x}. \tag{57}$$

In accordance with expressions (55) and (56) the pressure drop in the liquid and vapor regions of flow is given by

$$\Delta\overline{P}_L = Eu^{-1}\left\{(\overline{\rho}_{L,s} - 1) + \frac{\xi}{2Re_{L,0}}\int_0^{\overline{\ell}_L} \overline{v}_L \, d\overline{x}\right\}, \tag{58}$$

$$\Delta\overline{P}_G = Eu^{-1}\left\{(\overline{\rho}_{G,s,00} - 1)/\overline{\rho}_{G,s,0} + \frac{\xi}{2Re_{L,0}}\int_{\overline{\ell}_L}^{\overline{\ell}_G} \overline{v}_G \, d\overline{x}\right\}, \tag{59}$$

where

$$\overline{\rho}_{L,s} = \rho_{L,0}/\rho_{L,s}, \quad \overline{\rho}_{G,s,00} = \rho_{G,s}/\rho_{G,00}, \quad \overline{\rho}_{G,s,0} = \rho_{G,s}/\rho_{L,0}, \quad \overline{\ell}_i = \ell_i/d,$$
$$\Delta\overline{P}_L = 1 - \overline{P}_{L,s}, \quad \Delta\overline{P}_G = \overline{P}_{G,s} - \overline{P}_{G,00}.$$

Since $\int_0^{\overline{\ell}_L} \overline{v}_L \, d\overline{x} < [(1 + \overline{v}_{L,s})/2]\overline{\ell}_L$ and $\overline{v}_{L,s} < 1$, the following estimate of the maximum pressure drop in the liquid domain is valid:

$$(\Delta\overline{P}_L)_{max} \simeq \frac{\xi}{2Re_{L,0}Eu} \cdot \overline{\ell}_L. \tag{60}$$

The total pressure drop in a heated micro-channel is

$$\Delta\overline{P}_t = Eu^{-1}\left\{\frac{\xi}{2\mathrm{Re}_{L,0}}\left(\int_0^{\overline{\ell}_L} \overline{v}_L \, d\overline{x} + \int_{\overline{\ell}_L}^{\overline{\ell}_G} \overline{v}_G \, d\overline{x}\right) + (\overline{\rho}_t - 1) - We^{-1}\cos\theta\right\}, \tag{61}$$

where $\overline{\rho}_t = \rho_{L,0}/\rho_{G,00}$.

4. Stationary flow regimes

Rearranging the thermal balance equation (41) and using expressions (46)–(50) we arrive at

$$-\left\{\vartheta_L - Pe_L\frac{\vartheta_L\overline{\ell}_L - (\overline{T}_s - 1)}{1 - e^{-Pe_L\overline{\ell}_L}}\right\} + \lambda_{G,L}\cdot c_{pL,G}\vartheta_L\left\{1 - e^{-Pe_L\lambda_{G,L}(1-\overline{\ell}_L)}\right\} = JaPe_L, \tag{62}$$

where

$$\lambda_{L,G} = \lambda_L/\lambda_G,$$
$$c_{pL,G} = c_{pL}/c_{pG}.$$

The temperature distribution within the liquid and vapor domains of a heated micro-channel is plotted in Fig. 3. The liquid entering the channel absorbs heat from the walls and its temperature increases. As the liquid flow toward the evaporating front it reaches a maximum temperature and begins to decrease the temperature while heat transfers to the front from the liquid in order to establish the evaporation process. An increase of ϑ_L leads to shortening of the liquid domain as well as to a displacement of the point corresponding to the maximum temperature towards the inlet cross-section (Fig. 4). This process is accompanied by a decrease of the maximum liquid temperature and an increase of the heat losses in the inlet cross-section (Fig. 5). The effect of Pe_L on the length of the liquid domain is illustrated in Fig. 6. An increase of Pe_L leads to a decrease of $\overline{\ell}_L$. The liquid–vapor heat flux ratio at the evaporation front is shown in Fig. 7. An increase of the Peclet number is accompanied by an increase of $(q_L/q_G)_{\overline{x}=\overline{\ell}_L}$. This is due to the fact that when the vapor–liquid Peclet number increases two events occur: (i) more heat flux, at the front, is needed to evaporate a larger quantity of liquid, (ii) its influence on the temperature field, and thus on the temperature slope, diminishes. Since the vapor Peclet number is very large, compared to the liquid Peclet number, the contribution of the vapor domain to the front heat flux increases much slower than that of the liquid as the Peclet number increases, thus $(q_L/q_G)_{\overline{x}=\overline{\ell}_L}$ must increase.

Eq. (62) contains seven dimensionless parameters accounting for the hydrodynamic and thermal effects. The regimes in which stable flows in a heated capillary are possible correspond to the following interval of the length $\overline{\ell}_L : 0 < \overline{\ell}_L < 1$. The latter allows us to use Eq. (62) to define the domains of the existence of stable and unstable flow regimes. In the multi-dimensional parametric

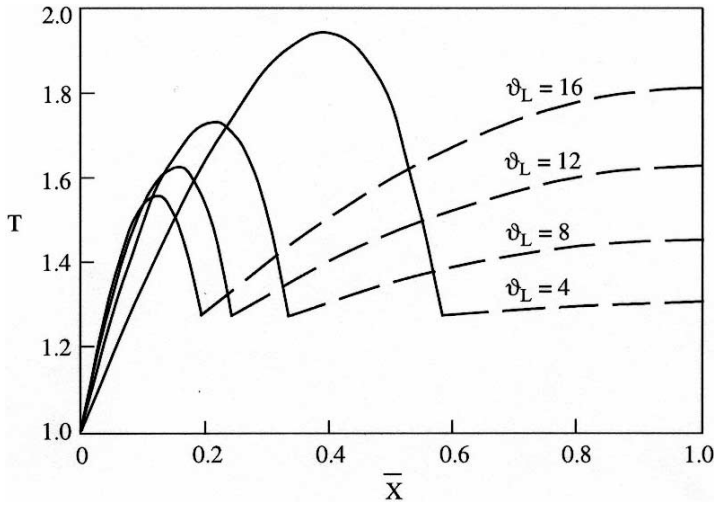

Fig. 3. Temperature distribution in a heated capillary. Solid line: liquid; dotted line: vapor (water at atmospheric pressure, $Pe_L = 6$, $Ja = 1.82$).

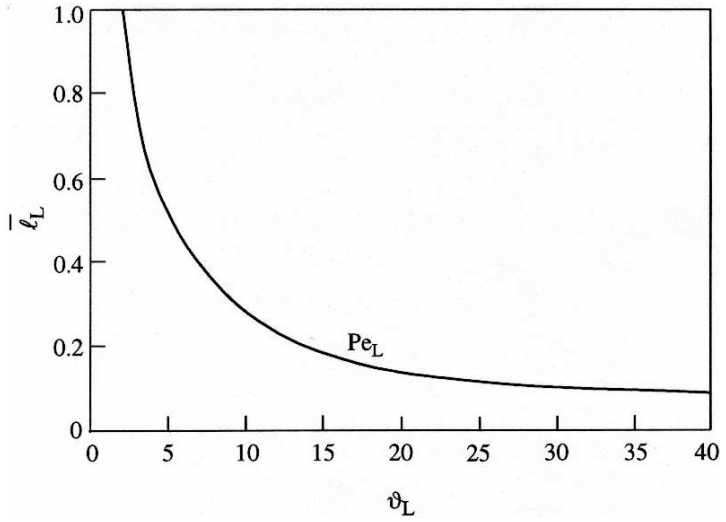

Fig. 4. The effect of ϑ_L on the length of liquid domain $\bar{\ell}_L$, for water and atmospheric pressure, $Ja = 1.82$ and $Pe_L = 6$.

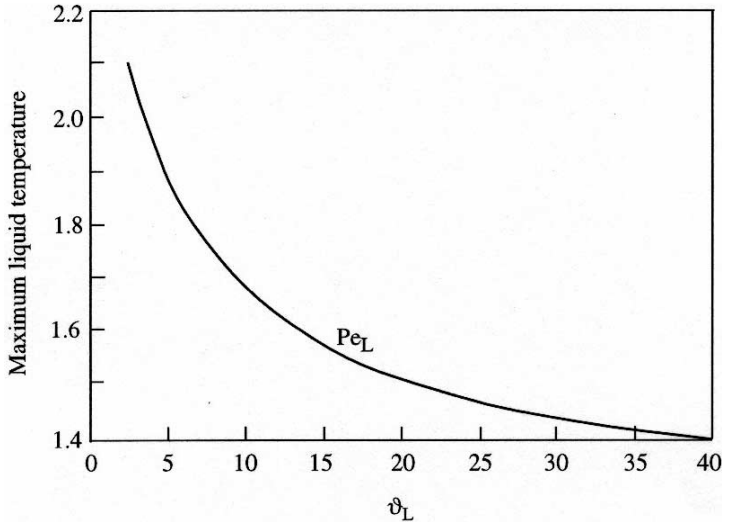

Fig. 5. Dependence of the maximal temperature on ϑ_L, for water at atmospheric pressure, $Ja = 1.82$ and $Pe_L = 6$.

space ($\bar{\ell}, \vartheta_L, Pe_L, Ja, \overline{T}_s, \lambda_{L,G}, c_{pL,G}$), the limiting values of these parameters correspond to a surface subdividing the parametric space into domains which correspond to various flow regimes.

The solution of Eq. (62) may be represented as 35 spatial (or 21 planar) diagrams which establish correlations between any three (or two, for the planar diagram) parameters when all the other parameters are fixed. These diagrams allow us to outline the domains of stable flow regimes and to determine the values of the parameters corresponding to the change between the stable and unstable flows.

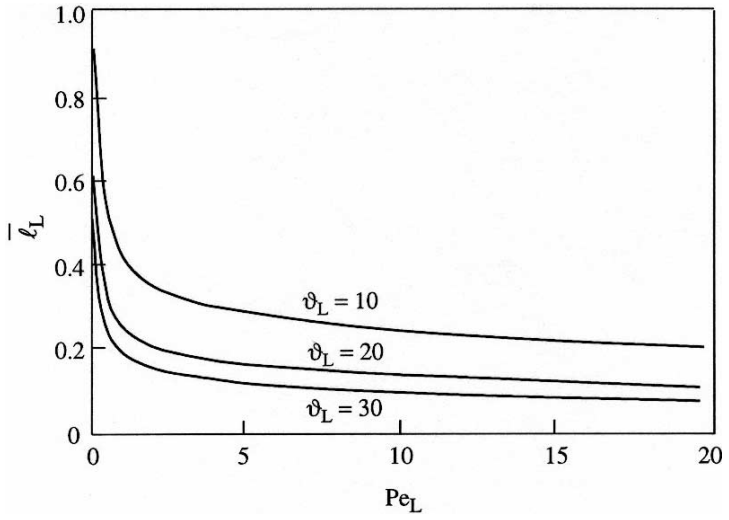

Fig. 6. The length of liquid domain as a function of Pe_L.

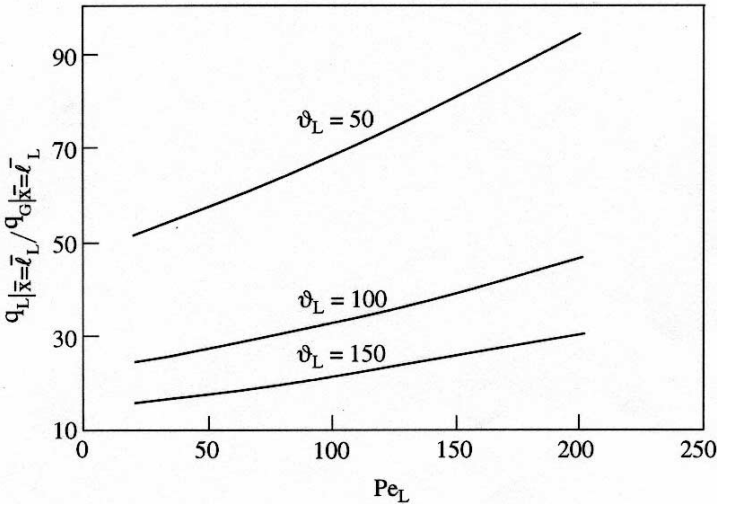

Fig. 7. The ratio $(q_L/q_G)_{\bar{x}=\bar{\ell}_L}$ versus the Peclet number (water at atmospheric pressure).

Consider some particular cases, which are of interest to the understanding of the general flow properties in a heated capillary. First, we examine a simple case when the Peclet number is much less than unity. Since $\bar{\ell}_L < 1$, the assumption $Pe_L \ll 1$ corresponds to the condition $Pe_L\bar{\ell}_L \ll 1$. In this case Eq. (62) reduces to

$$\bar{\ell}_L^2 - K_1\bar{\ell}_L + K_2 = 0, \tag{63}$$

where

$$K_1 = (\vartheta_L - Ja)/\vartheta_L, \quad K_2 = (\bar{T}_s - 1)/\vartheta_L Pe_L.$$

For any finite value of the parameters ϑ_L and Pe_L, it is seen that the dimensionless length of the liquid domain $\overline{\ell}_L$, cannot be equal to 0 and 1, since the term K_2 and the parameter Ja are positive. To determine a relationship between the parameters corresponding to the stable flow in the case $Pe_L \ll 1$, Eq. (63) should be solved to find $\overline{\ell}_L$

$$\overline{\ell}_L = 0.5\left(K_1 \pm \sqrt{K_1^2 - 4K_2}\right). \tag{64}$$

Since $\overline{\ell}_L$ should be positive, the physically realistic solution of Eq. (64) is possible only under the following conditions:

$$K_1 > 0, \tag{65}$$

$$K_1^2 \geqslant 4K_2. \tag{66}$$

From inequality (65) it follows that for

$$\vartheta_L > Ja \tag{67}$$

a steady flow is possible.

To estimate the range of possible variations of Pe_L and ϑ_L for a given $\overline{T}_s$ and Ja inequality (66) is presented in the following form:

$$Pe_L \geqslant 4\frac{(\overline{T}_s - 1)\vartheta_L}{(\vartheta_L - Ja)^2}, \tag{68}$$

where the equality corresponds to the low boundary of the stable flow domain.

The dependence $Pe_L = Pe_L(\vartheta_L)$ is shown in Fig. 8(a). Each point of this curve corresponds to a certain position of the evaporation front. Extreme points (the upper one $\overline{\ell}_L = 0$ and the lower one $\overline{\ell}_L = 1$) correspond to $\vartheta_L = Ja$, $Pe_L \to \infty$ and as $\vartheta_L \to \infty$ the Peclet number Pe_L tends to 0, respectively.

The domain of the stable flow is located to the right of the boundary $Pe_L(\vartheta_L)$ (the shaded region in the graph). To the left of this curve is the domain in which stable flows in a heated capillary cannot occur. Relation between the parameters ϑ_L and Ja, the parametric plane Pe_L–ϑ_L may be subdivided into two domains: (i) $\vartheta_L < Ja$, and (ii) $\vartheta_L > Ja$. Within the first of these the stable flows cannot occur at any values of the parameters Pe_L and $\overline{T}_s$. At $\vartheta_L > Ja$ various flow regimes may be realized: (i) a stable flow at $Pe_L > Pe_{Lb}$, and (ii) a unstable at $Pe_L < Pe_{Lb}$ (Pe_{Lb} is the value of the Peclet number corresponding to the boundary curve).

In the second case when ($Pe_L \gg 1, Pe_L\overline{\ell}_L \gg 1$), expression (62) reduces to

$$\overline{\ell}_L = (Pe_L\vartheta_L)^{-1}\{Pe_L[Ja + (\overline{T}_s - 1)] + \vartheta_L(1 - \lambda_{G,L}c_{pL,G})\} \tag{69}$$

Assuming $\overline{\ell}_L \leqslant 1$ in Eq. (69) we obtain

$$Pe_L \leqslant \frac{\vartheta_L(1 - \lambda_{G,L}c_{pL,G})}{\vartheta_L - [Ja + (\overline{T}_s - 1)]}. \tag{70}$$

The dependence $Pe_L = Pe_L(\vartheta_L)$ is shown in Fig. 8(b). The line $\vartheta_L = Ja + (\overline{T}_s - 1)$ divides the parametric plane Pe_L–ϑ_L into two domains: (i) an unstable flow regime domain for any value of $Pe_L[\vartheta_L < Ja + (\overline{T}_s - 1)]$, (ii) a stable flow regime domain $[\vartheta_L > Ja + (\overline{T}_s - 1)$ and

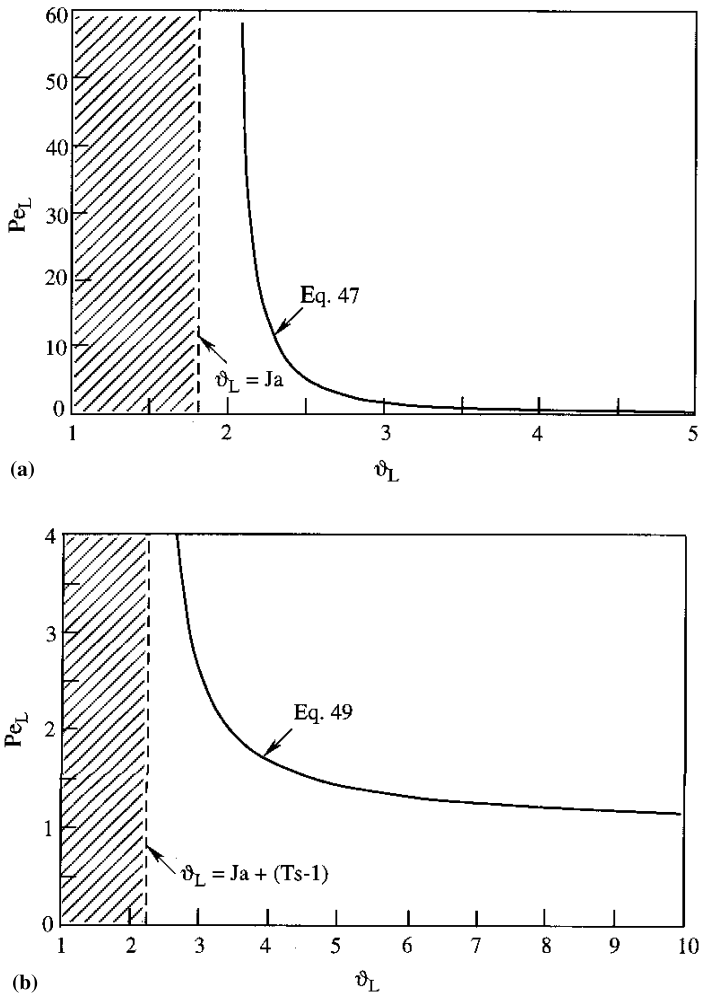

Fig. 8. The dependence $Pe_L(\vartheta_L)$. Shaded region: unsteady: (a) $Pe_L \ll 1$; (b) $Pe_L \gg 1$.

$Pe_L < 1 - \lambda_{G,L}c_{pL,G}]$. Thus, at $Pe_L \gg 1$ the domain of stable flows in a heated capillary with a distinct evaporation front is restricted by the lines $\vartheta_L = Ja + (\overline{T}_s - 1)$ and $\mathrm{Pe}_L = 1 - \lambda_{G,L}c_{pL,G}$. Note that the last restriction had already been met by the restriction $Pe_L \gg 1$.

5. Experimental facility and experimental results.

The experimental set up is shown in Fig. 9. Prior to the experiment, the water was passed through a 1/2 μm cartridge filter, to fill up the reservoir. Water was circulated through the flow loop by a peristaltic pump (6). As the fluid leaves the reservoir (10), it passes through a silicon rubber tube and then flows into the test module (1) and leaves its through the outlet silicon rubber tube. A special Teflon cartridge was manufactured to hold the module in place and to move it in

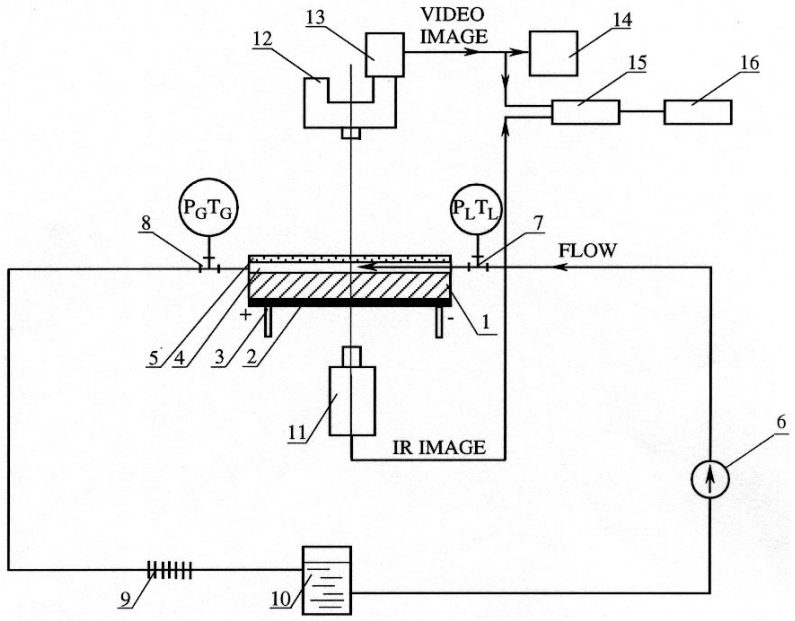

Fig. 9. Experimental set up: (1) test module; (2) heater; (3) electrical contact; (4) micro-channel; (5) Pyrex; (6) peristaltic pump; (7)–(8) pressure and temperature measurements; (9) cooler; (10) reservoir; (11) IR camera; (12) microscope; (13) high speed video camera; (14) PC; (15) synchronizer; (16) video recorder.

the x–y plane. The temperature and pressure were measured at both the inlet (7) and exit (8) of the test section using a 0.3 mm copper–constantane thermocouple and silicon pressure gauges, respectively. The thermocouples and pressure gauge output voltages were recorded by multi-scan data acquisition module, which in turn was connected to a PC via a data acquisition card. The input voltage was then translated to °C and kPa by a calibration process prior to the test runs.

A DC power supply with an operating range of 0–60 V was used to supply power to the chip aluminum resistor (2). The Teflon module cartridge was placed underneath a high speed CCD camera (13) mounted on a microscope (12), which photographed the boiling process occurring in the micro-channel (4) to the PC (14) and a video recorder (16). At the same time an IR (11) camera measured the resistor's temperature on the other side of the chip. Special software was used to analyze the IR results and to compute the average and maximum temperature on the chip.

The test module is shown in Fig. 10. The device of micro-channel silicon substrate is shown in Fig. 11. It consists of some parts: the first and most important is a 525 μm micro-channel silicon substrate (1) bonded to the 500 μm Pyrex cover (5) and the last is the flow manifold. The micro-channel silicon substrate was fabricated by photolithography process on one side and consists of 16 mm long triangular micro-channels (4) having hydraulic diameter ranging from 50 to 200 μm. On the other side of a 1×1 cm^2 aluminum resistor, silicon substrate was evaporated, forming three distinct channel regions; inlet adiabatic, heat flux dissipation and outlet adiabatic. The channels side were glued to a Pyrex substrate by anodic bonding to form the chip test module.

While the manifolds were fabricated by plain molding process, the micro-channels substrate fabrication was quite complicated and was achieved by a multi-stage process. The following main

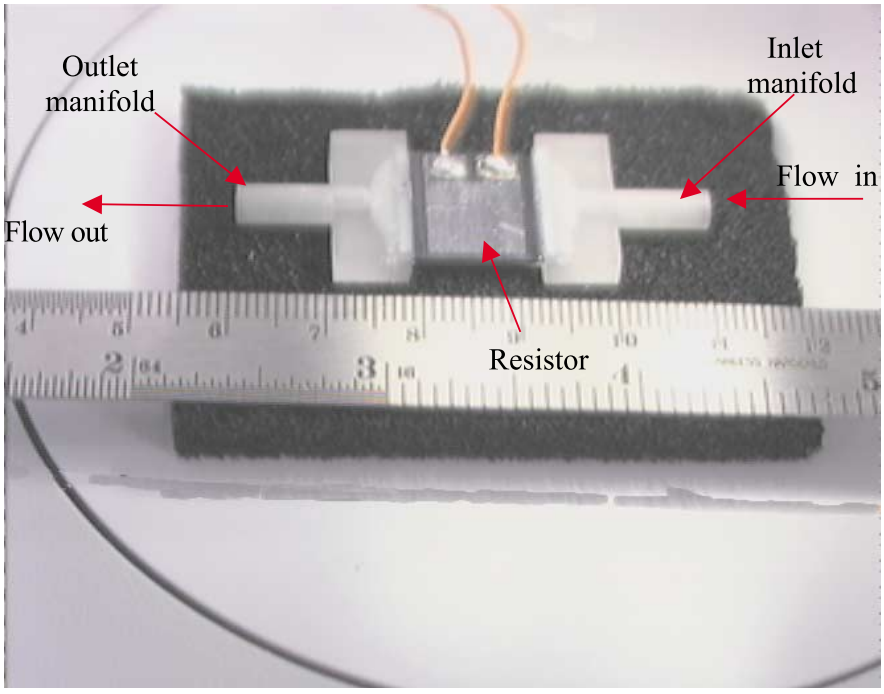

Fig. 10. The test module.

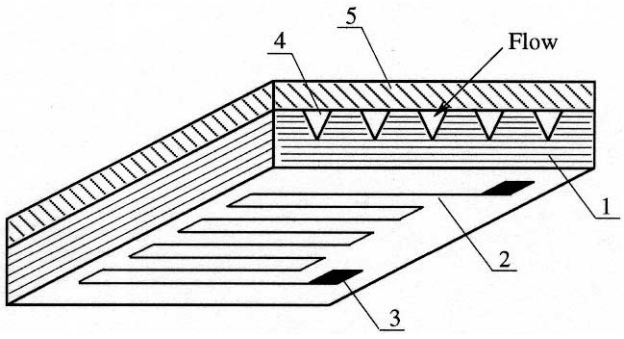

Fig. 11. The micro-channel silicon substrate bonded to the 500 μm micro-channel cover Pyrex: (1) test module; (2) heater; (3) electrical contact; (4) micro-channel; (5) Pyrex.

stages were used in the process: (i) double side oxidation of a 525 μm ⟨1 0 0⟩ silicon substrate to 1000 Å, (ii) single side 1200 Å silicon nitride deposition, (iii) silicon nitride channels template opening by reactive ion etching (RIE), (iv) channels template oxidation buffer oxide etching (BOE), (v) silicon etching by tetramethyl ammonium hydroxide (TMAH), (vi) 4000 Å double side oxidation, (vii) silicon nitride etching by RIE, (viii) 1000 Å oxidation layer etching, (ix) silicon/Pyrex anodic bonding, (x) aluminum thin film evaporation, (xi) aluminum template etching and (xii) wafer sawing.

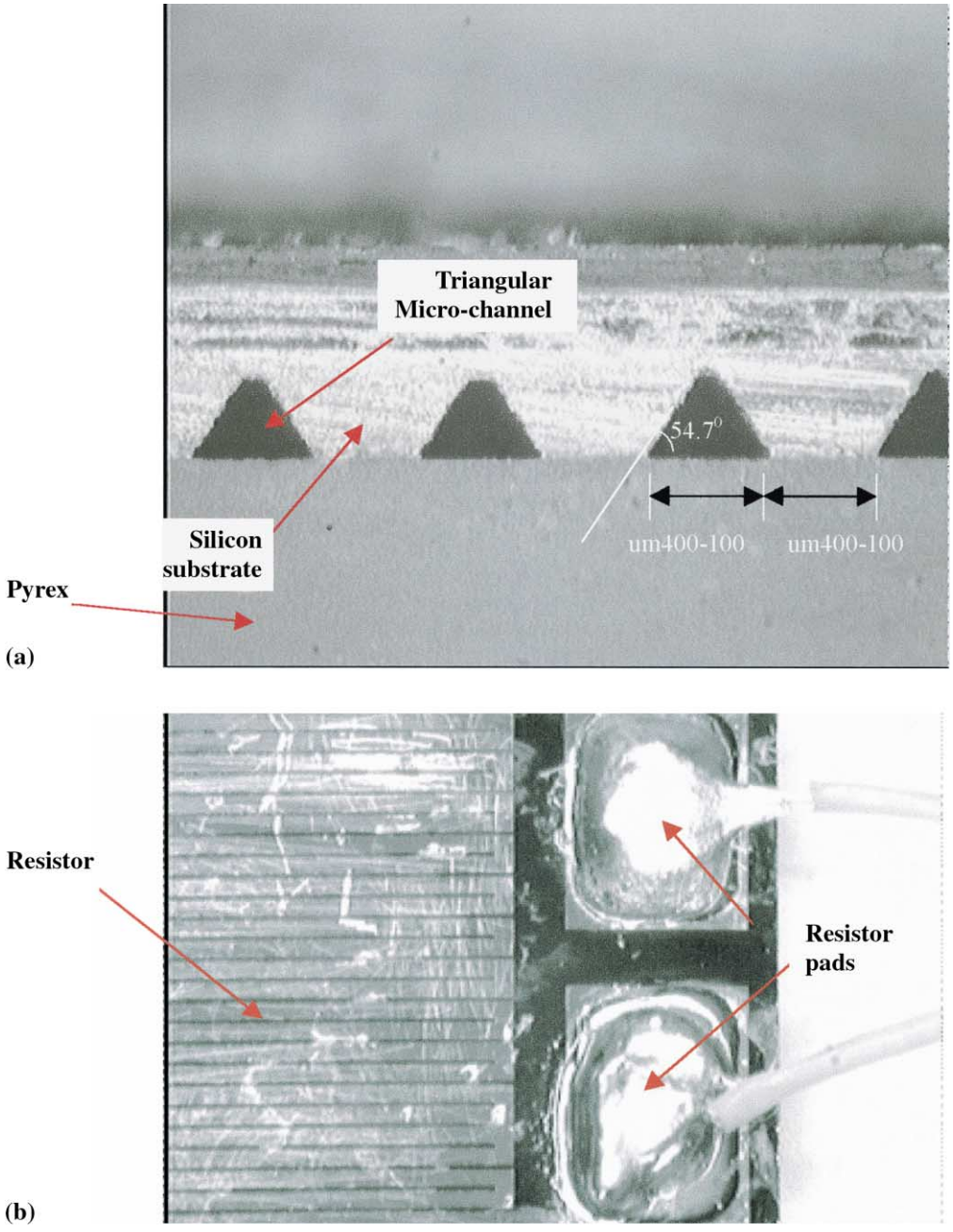

Fig. 12. The (a) triangular micro-channels, (b) unpainted resistor.

Once the micro-channels were fabricated, the manifold were bonded to the substrate to epoxy glue, and the resistor was wired by silver-based epoxy electric conductor and painted by 1 μm thin pain to increase the surface emissivity. The triangular micro-channels and the unpainted resistor are shown in Fig. 12.

The experiments were conducted on a heat exchanger described above, having 17 triangular micro-channels with hydraulic diameter of 157 μm and mass flow rates of 5.7 ml/min. The applied heat flux ranged from up to 35 W/cm^2. The deviation of q^* from its nominal value does not exceed 0.5%. The characteristic value of the dimensionless groups at which the observations were carried out are: $Eu \sim 10^6$, $Pe_L \sim 7 \times 10^2$, $\vartheta_L \sim 0.3$, $Ja \sim 1.8$. That allows us to study the flow in a heated capillary outside the domains of the steady flows.

(a)

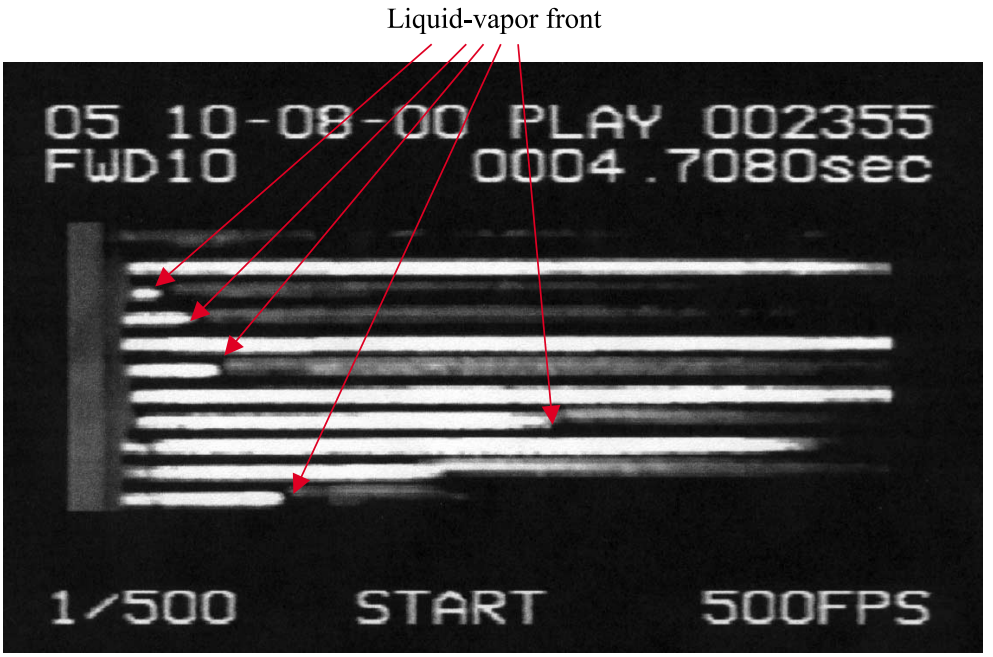

(b)

Fig. 13. Flow types in a heated capillary: (a) bubble formation; (b) liquid–vapor front.

The experimental results show that the evaporating mechanism in two-phase flows in micro-channels differ considerably from larger sized channels. Two distinct phase domains, one for the liquid and another for the vapor, were observed, with a very short (in the order of the hydraulic diameter) section of two-phase mixture between them. This implies that the outlet vapor mass quality for a steady flow can take only the values of 0 (single-phase liquid flow) or unity (saturated or superheated vapor). The energy required for the flow with zero outlet quality is much lower than the energy required for the quality larger than one. Thus an energy gap is found between those energy levels, for which steady evaporating two-phase flow does not exist. If the applied heat flux is sufficient to initiate evaporation at quality lower than one an unsteady flow is expected with an outlet phase flow fluctuation corresponding to some time-average mass quality lower than one, as was shown to be the case in the present experiment. This agrees well with the theoretical model results since it lies in the unsteady flow region ($\vartheta_L < Ja + (\overline{T}_s - 1)$) as can be seen in Fig. 8(b).

The development of the two-phase flow in a heated capillary at different Peclet number is illustrated in Fig. 13. It shows that different mechanisms of two-phase flow formation may occur depending on the value of Pe_L. At small Pe_L the fine bubbles formation (on the micro-channel wall) plays a dominant role. Growth of these bubble leads to a blockage of the micro-channel, to a sharp change of the hydraulic resistance and ultimately to an unsteady gas–liquid flow. This effect is negligible at large Peclet number. In this case liquid evaporation is accompanied by formation

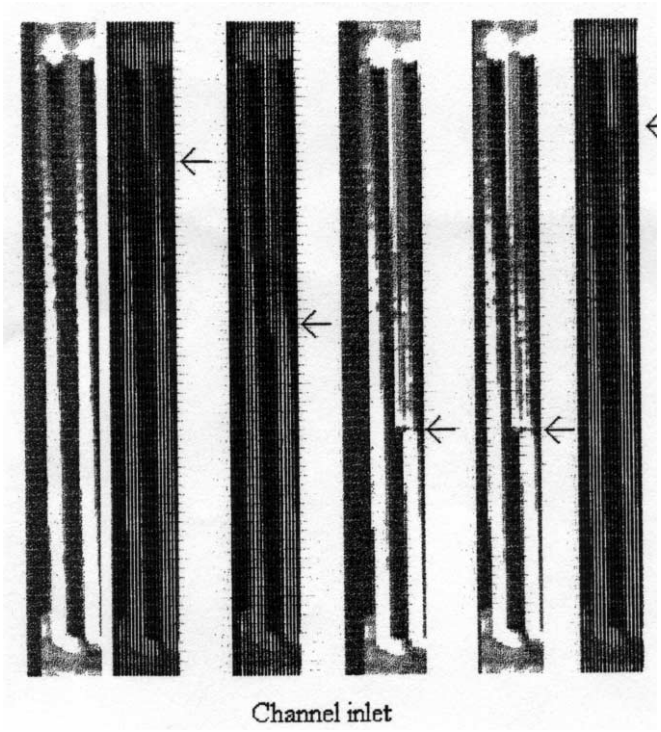

Fig. 14. Unsteady flow in a heated capillary: $\vartheta_L = 0.3$; $Ja = 1.83$; $Pe_L = 598$.

of the two-phase flow with distinct vapor–liquid evaporation front dividing the domains of the liquid and the vapor. Depending on the values of the governing parameters such flow may be steady or unsteady. A particular flow at $Pe_L \approx 500$ and $\vartheta_L \approx 0.3$ (the conditions correspond to boundary of the unsteady flow domains) are shown in Fig. 14. A number of successive photos of the flow are presented. They show that the position of the evaporation front changes during the periodical observation. Thus at the given values of parameters the flow in a heated capillary is non-steady. The latter agrees with the estimation of the boundary of steady states given in Section 4.

6. Conclusion

In the present paper a simplified one-dimensional approach to study two-phase flow in a heated micro-channel was developed. This approach was used to study the steady flow regimes as well as to determine the boundary of the steady flow domains. The effect of a number of dimensionless parameters (Pe, Ja, ϑ, etc.) on velocity, temperature and pressure distributions within the domains of liquid or vapor has been studied. The experimental investigation of the flow in a heated capillary was carried out. It has been shown that, depending on the value of the Peclet number, various types of the process occurred. At small Pe_L, the dominant role is the bubble formation at the channel wall, whereas for $Pe_L \gg 1$, liquid evaporation leads to formation of an evaporation front.

The experimental results also demonstrated that evaporating two-phase flow in micro-channels with time-average mass quality lower than one is unsteady. This result agrees well with the one-dimensional model prediction. Physically this flow regime can be explained by the special mechanism associated with the micro-channel geometry, which appear to have two distinct phase domains: one for the liquid and the other for the vapor, with a very short section of two-phase mixture between them. It follows that the outlet flow can exhibit only single-phase, either liquid or vapor. Thus, a vapor mass quality lower than 1 means alternating outlet phase with a time-average quality lower than one.

Acknowledgements

This work was supported by the Ministry of Science and the Arts (State of Israel). L.P. Yarin is supported by the Israel Council for Higher Education.

References

Bowers, M.B., Mudawar, I., 1994. High flux boiling in low flow rate, low pressure drop mini-channel and micro-channel heat sink. Int. J. Heat Mass Transfer 37, 321–332.

Hsu, Y.Y., 1962. On the size range of active nucleating cavities on a heating surface. J. Heat Transfer 184, 207–213.

Incropera, F.P., 1999. Liquid Cooling of Electronic Devices by Single-phase Convection. Wiley, New York.

Katto, Y., 1978. A generalized correlation for critical heat flux for the forced convection boiling in vertical uniformly heated round tubes. Int. J. Heat Mass Transfer 21, 1527–1542.

Khrustalev, D., Faghri, 1995. Fluid flow effect in evaporation from liquid–vapor meniscus. J. Heat Transfer 118, 725–730.

Kuchling, H., 1980. Nachschlagebücher für Grundlagenfächer, Physik. Verb. Fachbuchverlag, Leipzig.

Landau, L.D., Lifshitz, E.M., 1959. Fluid Mechanics. Second ed., Pergamon, London.

Peles, Y.P., Yarin, L.P., Hetsroni, G. 1998, Heat transfer of two phase flow in a heated capillary, Heat transfer 1998. In: Proceedings of the 11th International Heat Transfer Conference Vol. 2, Kyongju, Korea, p. 193–198.

Peng, X.F., Wang, B.X., 1993. Forced convection and flow boiling heat transfer for liquid flowing through micro-channels. Int. J. Heat Mass Transfer 36, 3421–3427.

Peng, X.F., Wang, B.X., 1998. Forced convection and boiling characteristics in microchannels. 1998, Heat Transfer 1998. In: Proceedings of the 11th IHTC, Vol. 1, p. 371–390.

Peng, X.F., Wang, B.X., 1994a. Cooling characteristics with micro-channeled structures. J. Enhanced Heat Transfer 1, 315–326.

Peng, X.F., Wang, B.X., Peterson, G.P., Ma, H.B., 1994b. Experimental investigation of heat transfer in flat plates with rectangular micro-channels. Int. J. Heat Mass Transfer 37, 127–137.

Peng, X.F., Peterson, G.P., Wang, B.X., 1996. Flow boiling in binary mixtures in micro-channels plates. Int. J. Heat Mass Transfer 39, 1257–1263.

Peng, X.F., Hu, H.Y., Wang, B.X., 1998. Boiling nucleation during liquid flow in micro-channels. Int. J. Heat Mass Transfer 41, 101–106.

Tukermann, D.B., Pease, R.F.W., 1981. High performance heat sink for VLSI. IEEE Electron Device Lett. EDI 2, 126–129.

Yamagata, Hironai, F., Mishikawa, K., Matsouka, H., 1955. Nucleate boiling of water on the horizontal heating surface. Memoirs of the Faculty of Engineering, Vol. 15, p. 98, Kyushu University, Japan.